

Revisiting Single-gated Mixtures of Experts

Amélie Royer¹

royer@qti.qualcomm.com

Ilija Karmanov^{1,2}

ikarmano@qti.qualcomm.com

Andrii Skliar¹

askliar@qti.qualcomm.com

Babak Ehteshami Bejnordi¹

behtesha@qti.qualcomm.com

Tijmen Blankevoort¹

tijmen@qti.qualcomm.com

¹ Qualcomm AI Research

Science Park 400

Amsterdam

The Netherlands

² Now working at NVIDIA Switzerland

Abstract

Mixture of Experts (MoE) are rising in popularity as a means to train extremely large-scale models, yet allowing for a reasonable computational cost at inference time. Recent state-of-the-art approaches usually assume a large number of experts, and require training all experts jointly, which often lead to training instabilities such as the router collapsing. In contrast, in this work, we propose to revisit simple single-gate MoE, which allows for more practical training. Key to our work are (i) a base model branch acting both as an early-exit and an *ensembling regularization* scheme, (ii) a simple and efficient *asynchronous* training pipeline without router collapse issues, and finally (iii) an automatic *per-sample* clustering-based initialization. We show experimentally that the proposed model obtains efficiency-to-accuracy trade-offs comparable with other more complex MoE, and outperforms non-mixture baselines. This showcases the merits of even a simple single-gate MoE, and motivates further exploration in this area.

1 Introduction

Neural networks are designed to extract a fixed set of exhaustive features for any given image. However, images exhibit varying levels of complexity, from simple cases such as single objects on a white background to images with clutter and difficult camera angles. Treating both of these cases equally can be wasteful from an efficiency perspective: This intuition has given rise to very active research in the fields of conditional computing [9] and early-exiting [10, 11, 12]. In conditional computing, subparts of the network are turned on or off dynamically based on the input image. This allows to increase the network's capacity at training time without affecting the computational cost at inference. The same conditional behavior applies in early exiting but across the depth dimension: The prediction can be finalized early in the network for simple images, avoiding unnecessary further computing.

In particular, Mixture of Experts (MoE) have gained a lot of traction in recent years for conditional computing. For instance, transformers with a massive number of parameters

are now becoming the new normal for natural language processing [1, 2, 3, 4]. Similar models are also starting to emerge in computer vision, leveraging extremely large datasets and numerous routing decisions [5]. The success of these large-scale conditional models begs the question whether similar results are also achievable for datasets and architectures of a smaller scale, more commonly used by practitioners (e.g. ResNet-18 on ImageNet). In this work, we introduce three ingredients to make simple single-gate MoE competitive with other state-of-the-art MoE, across a variety of architectures and dataset sizes. In particular, our training pipeline remains efficient and stable in all cases, in contrast to more complex dynamic routings [6], and avoids introducing new ad-hoc losses [7]. Specifically, we make the following contributions:

- In [Section 2.2](#), we introduce a single-gate MoE that consistently outperforms its non-mixture counterparts on various architectures. A key improvement in our proposed model is a *base network* branch whose features facilitate the initial expert selection. We also show that this base model acts as an excellent regularizer when ensembled with specialized experts, improving the overall performance.
- In [Algorithm 1](#), we also formulate a *simple and efficient* training procedure for the model, which is both stable and asynchronous. These results indicate that simple single-gate MoE is a promising direction to enable conditional computing for both small training- and inference- computational budgets.
- Finally, in [Section 2.3](#), we propose and evaluate a simple threshold rule to dynamically adapt the computational budget at inference, without retraining, which combines early-exiting through the base model and selecting a dynamic number of experts per sample.

2 Proposed Model

2.1 The Mixture of Experts Setup for Image Classification

A Mixture of Experts (MoE) consists of a set of K experts, $(e_k)_{1..K}$, each outputting a distribution over the target classes; The execution of these experts is conditioned by the *gate* g (or *router*), which outputs a probability distribution over the set of experts. The total likelihood of the model on the training dataset \mathcal{D} , which we want to maximize, is expressed as:

$$\mathcal{L}(\mathcal{D}) = \mathbb{E}_{(x,y) \sim \mathcal{D}} \left[\sum_{k=1}^K g(k|x) e_k(y|x) \right] \quad (1)$$

A successful MoE relies on the gate learning a decomposition of the input space across K clusters, such that experts specialize on the resulting subsets; The key underlying assumption is that this compositional approach outperforms a single model trained on the entire dataset. At inference time, the gate is thresholded, such that only one - or few - experts are executed, to control the accuracy/efficiency trade-off. Unfortunately, the standard MoE suffers from three major issues: **(i)** Because the experts only have a local view of the training set, regulated by the gate, their mixture is more prone to overfitting than a single model trained on the whole dataset [8]. **(ii)** Jointly training the gate and experts raises a chicken-and-egg problem: The gate has to route samples to the experts most likely to classify them successfully, but weaker experts need data to improve. This problem often leads to the gate collapsing, i.e., only feeding input samples to very few experts, which defeats the purpose of using an MoE in

the first place. **(iii)** The initial data subsets defined by the gate strongly influences the expert training. Thus, a naive random initialization may even further worsen the gate collapse issue if, for instance, an expert is heavily favored over others at initialization.

In this work, we propose two key changes to the MoE framework to alleviate the aforementioned issues and improve performance of simple single-gate MoE models. **First**, we introduce a novel generic knowledge branch, which we refer to as the *base model*: This module is trained on the whole dataset, and we use it **(i)** to tackle potential overfitting: It acts as a form of regularization for the experts by ensembling their outputs with this initial base prediction; **(ii)** to initialize the gate, using the feature space induced by the base model for clustering the training samples. and **(iii)** as an early-exiting branch that avoids executing any expert when not necessary, and is conditionally activated based on the input image. **Second**, we describe a simple, lightweight training scheme that first initializes the experts’ subsets by clustering the base model’s embeddings and then keeps the gate and experts independent during training in order to avoid the gate collapse issue.

In [Section 2.2](#), we describe the proposed model’s key components and training scheme; The model architecture is summarized in [Figure 1](#). Then, in [Section 2.3](#) we describe a simple conditional computing mechanism to obtain even more computationally-efficient models.

2.2 Model Summary

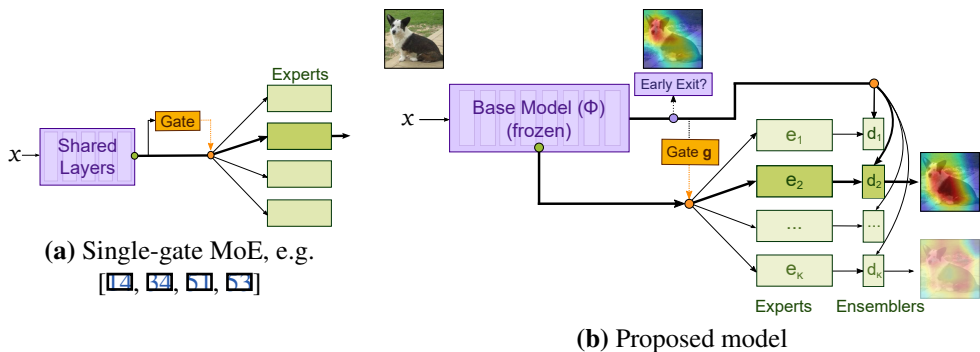


Figure 1: (left) MoE define a gate, g , that selects (●) which expert to execute based on the current representation (●) of input x . At inference, a unique expert is picked (in **bold**). (right) our proposed architecture maintains a full-depth base model, ϕ , which is (i) ensembled with the expert output, (ii) used as inputs to the experts and gate, and (iii) acts as an early exit (●) at inference. Grad-CAM [14] visuals reveal that the selected expert focuses on fine-grained details, while the base model attends to general features. The other non-selected experts produce poorly focused activation maps.

Architecture. The **base model** ϕ is a simple, ideally lightweight, network trained on the whole dataset, and is executed for every input. Its purpose is multi-fold: First, it is ensembled with the selected expert. While previous works [14, 51] often ensemble specialized experts together in MoE, we show in our experiments that ensembling one expert with this non-specialist branch is consistently more beneficial. Second, the base model acts as an early exit output at inference time, avoiding redundant expert computations for the easier samples (see [Section 2.3](#)). Finally, we reuse the early layers of the base model as inputs to the gate and the experts which allows us to reduce computational load even further.

The **gate** g is a simple linear layer taking as input the pre-logsits of the base model. At training time, it outputs a probability distribution over experts, $g(k|x)$, allowing for direct

backpropagation through these weights. At inference, we only select and execute the most probable expert, i.e., $g_{\text{test}}(k|x) = \mathbb{1}(k = \arg \max_{k'} g(k'|x))$; $\mathbb{1}(\cdot)$ being the indicator function. We also discuss in [Section 2.3](#) how we can dynamically select the number of active experts, rather than always defaulting to the top-1 expert.

Experts are neural networks whose input is an intermediate feature map of the base model. This design choice yields two benefits: **(i)** The experts' early features are shared and frozen, which reduces the number of trainable parameters and reduces the risk of experts overfitting (in particular when training on small datasets); and **(ii)** this allows the model to reuse computations from the base model at inference time, further improving efficiency.

Finally, **ensemblers** are shallow neural networks, one for each expert, combining outputs of the base model and the expert selected by the gate. We experiment with both stacking and bagging ensembling methods. In the text, we also refer to $e'_k(y|x) = d_k(\phi(y|x); e_k(y|x))$ as the classification output of the ensembler d_k , which ensembles the k -th expert and base model ϕ .

Training Procedure. We summarize our asynchronous training scheme in [Algorithm 1](#), in which the gate and experts are trained independently in parallel. This training procedure relies on three key insights: **First**, to avoid gate collapse, we keep the gate weights fixed while training the experts. This makes the model heavily dependent on the gate initialization. Thus, to define a meaningful initial gate g_0 , we cluster the pretrained base model's embeddings using K -means [[29](#)]. A similar initialization scheme has been used in the hierarchical classification literature [[12](#), [52](#)]; In contrast, we do not restrict this initial clustering step to be a hard assignment to a unique expert, nor to be on a per-class basis.

A **second** issue stems from uncalibrated outputs [[13](#), [53](#)]: Training an ensembler d_k jointly with its expert e_k often leads to d_k heavily favoring the base model, preventing the expert from specializing. This behavior is likely due to the base model being overly confident on many training samples: In fact, this is particularly apparent on small datasets where the base model is already close to perfectly fitting the training set, e.g., on CIFAR-100. To avoid this problem, we only start training d_k *after* fully training the corresponding expert e_k .

Thirdly, because the experts are initialized with the base model's pretrained weights, but are then trained on a specialized subset of the data given by the gate, they might "forget" classes they never see. This is similar to *catastrophic forgetting* [[12](#), [53](#)]. While the proposed ensemblers partially alleviate this issue by providing additional regularization, we find that it is often beneficial to also route non-assigned samples the experts: Specifically, in step 4 and 5 of [Algorithm 1](#), the gate g_0 is "smoothed" using the transformation: $\Gamma : \cdot \mapsto \text{clip}(\cdot, \gamma, 1)$, where γ is a hyperparameter. We experimented with **(i)** using the smoothed gate weights to re-weight the loss of all samples, including negative ones (as portrayed in [Algorithm 1](#)) or **(ii)** using these gate weights as sampling probabilities when forming the training batch. Both yield similar results, and while **(i)** is simpler to implement, we find that **(ii)** is more practical for large datasets, as it often leads to faster convergence, hence reduced training times.

An alternative joint training scheme. We also consider extending the training scheme to handle joint end-to-end training of the gate and experts by using the Expectation Maximization (**EM**) algorithm [[8](#)] to alleviate the "chicken-and-egg" problem. EM alternates between two steps: **(E)** computing new gate weights, updated based on the current experts' performance, and **(M)** separately training the experts according to this new assignment, while forcing the gate to match it. Taking into account training costs, it is beneficial to keep a low number of **E** steps (N_E) as every update of the posterior requires synchronization across all experts. In fact, one can show that [Algorithm 1](#) is equivalent to setting $N_E = 0$. In prac-

Algorithm 1 Proposed asynchronous training scheme**Require:** Training dataset \mathcal{D} , base model ϕ , gate g , experts $e_{1\dots K}$, ensemblers $d_{1\dots K}$ 1. Train the **base model** ϕ on dataset \mathcal{D} (or use an off-the-shelf pretrained model)2. Cluster the base model embeddings using K -means, obtaining centroids $c_{1\dots K}$ Define the **initial gate** $g_0 : (x, k) \mapsto m(\phi(x), c_k)$ where m is a similarity function and is such that the weights across clusters sum to 1 for a given sample x .3. Train the **gate** g by minimizing the KL divergence $\text{KL}(g_0, g)$ **for** $k = 1$ to K (in parallel) **do**Initialize the k -th expert from the base model’s weights: $\theta_{e_k} \leftarrow \theta_\phi$ 4. Train **expert** e_k following (1), i.e., by maximizing $\sum_{(x,y) \sim \mathcal{D}} g_0(k|x) e_k(y|x)$ 5. Train **ensampler** d_k by maximizing $\sum_{(x,y) \sim \mathcal{D}} g_0(k|x) d_k(\phi(y|x); e_k(y|x))$ **end for**

tice, we observe that larger values N_E can lead to higher accuracies (e.g., on tiny-ImageNet: **+1.37%** without ensemblers, and **+0.43%** with ensemblers). However, the improved performance is often not worth the higher training costs, hence we only report results using **Algorithm 1** in our experiments section. We describe the derivation of the EM variant and experiments in more details in the **supplemental material**.

2.3 Anytime Inference via Early-Exiting and Dynamic Ensembling

By design, our framework integrates a straightforward option for early-exiting by directly outputting the base model’s predictions in easy cases, to improve computational efficiency further. Following previous early-exiting literature [49, 53, 50], our model decides whether to early-exit or to execute the gate-selected expert by thresholding the base model’s confidence at inference time. We also consider other early-exit designs in the **supplemental material**. Additionally, it is clear from Equation 1 that MoE can be viewed as an ensemble of experts weighted by the gate, rather than using only the top-1 expert as is usually done for efficiency purposes. Similar to [50], we propose to threshold the gate outputs to determine which experts to include dynamically at inference. In order to combine both the early-exiting and expert ensembling behaviors under a unique thresholding rule, we introduce the quantity $\alpha_k(\mathbf{x}) = \mathbf{g}(\mathbf{k}|\mathbf{x})(1 - \max_y \phi(\mathbf{y}|\mathbf{x}))$. From a probabilistic perspective, $\alpha_k(x)$ can be interpreted as the joint probability that the sample x is not early-exited, *and* that the gate routes x to the k -th expert. Intuitively, if this quantity is below a certain threshold for all experts, it means that the base model has a high confidence and the gate does not confidently route the sample to any expert; thus we should early exit. Thus, given a trained gate g and experts (with their ensemblers) e'_k , we define the **anytime model** $p^{\text{at-}\tau}$, which combines both early-exiting and dynamic experts ensembling, as follows:

$$ee(x) = 1 \text{ iff } \forall k \in [1, K], \alpha_k(x) < \tau \quad (2)$$

$$p^{\text{at-}\tau}(y|x) = ee(x)\phi(y|x) + (1 - ee(x)) \sum_{k=1}^K \mathbb{1}(\alpha_k(x) \geq \tau) g(k|x) e'_k(y|x) \quad (3)$$

where $\mathbb{1}(\cdot)$ is the indicator function, and $\tau \in [0, 1]$ is a hyperparameter. We show in experiments that varying τ allows the model to quickly achieve a wide range of computational budgets at inference time, without any retraining.

3 Related Work

Conditional computing aims to learn a sparse connectivity pattern conditioned on the input sample. To achieve such pattern, many works add a mixture of expert layers at several stages throughout the network [6, 11, 61, 69, 47, 48, 52]. Unlike single-gated MoE, the increased number of routing decisions incurs some practical drawbacks: (i) At inference, a new submodel has to be loaded in memory for every routing decision, which becomes increasingly cumbersome as the number of gates increases and (ii) all gates and experts have to be trained synchronously which leads to huge models to train and training instabilities. This often leads to complex training pipelines, e.g. relying on reinforcement learning [6, 69, 47] to learn the routing mechanism. More recently, [53] has proposed a simpler k-means-like routing mechanism that evolves during training via moving average. However, they also report that the training pipeline requires large batch sizes, and is prone to mode collapse.

Simpler **single-gate mixture of experts** have also been successfully applied to neural networks for various applications such as image classification [10], detection [24], retrieval [14] and scene recognition [20]. More recently, [53] has shown that such models can achieve significant accuracy/efficiency gains in the large-scale regime. However, their training pipeline relies on several unclear heuristics. Orthogonal to these, hierarchical classification is a subclass of MoE, in which the routing is learned on a *per-class* basis, aiming to route all samples of a ground-truth class to the same expert. Several works [4, 13, 60, 65] directly leverage an external class taxonomy (such as WordNet [62]). A follow-up line of thought extracts such information from a pretrained classifier [64, 51], or even learns the optimal taxonomy jointly with the image representations [9, 28]. Such models have been shown to improve the efficiency/accuracy trade-off in classification tasks. However, this class-based routing is a limiting assumption, and per-sample routing has been shown to outperform hierarchical classification models when correctly parametrized [10, 20].

Finally, MoE can be seen as an **ensembling** technique whose weights are learned by the gate. While it is common to assume each sample is routed to a unique expert to maximize efficiency, some works [14, 64, 51] have considered combining several experts to boost accuracy. In contrast, we show that combining one specialized expert with the generic knowledge base model with simple ensemble methods such as averaging or linear stacking [44] is generally more efficient than ensembling multiple specialized experts.

4 Experiments

We perform experiments on datasets of different scales: CIFAR-100 [23], tiny-ImageNet [26] (a downsampled subset of ImageNet with 200 classes and 110k images), and ILSVRC2012 [42].

We use ResNets [16] with different depths as our main backbone architecture. For CIFAR-100 and tiny-ImageNet, we use a modified variant of ResNets which eliminates the first two downscaling operations (strided convolution and max-pooling), commonly used in the literature [21, 46, 52]; We dub it “*tiny-ResNet*” or **tr** for short. We follow previously established training pipelines to train our baseline models, specifically [6] for CIFAR-100 and [27] for tiny-ImageNet.

For ImageNet, we additionally perform experiments on MobileNetv3-small [17], and use the standard checkpoints provided in torchvision’s model zoo [66] as base models. In all of our experiments, we initialize the experts with pretrained weights from the base model and train them with the same hyperparameters and data augmentations as the baseline, although

Base Model	Expert	top-1 acc	MACs (x 1e9)		#params x 1e7	
			inference	trainable	inference	trainable
tr18 baseline	-	77.95	0.56	1.12	1.12	
tr10	tr10	77.96 ± 0.20	0.37	0.96	9.29	
	tr18	78.78 ± 0.22	0.52	1.55	21.1	
tr34 baseline	-	78.60	1.16	2.13	2.13	
tr18	tr10	79.78 ± 0.05	0.67	1.58	9.29	
	tr18	79.90 ± 0.22	0.82	2.17	21.1	
tr50 baseline	-	80.10	1.30	2.37	2.37	
tr34	tr10	80.48 ± 0.17	1.28	2.59	9.29	

Base Model	Expert	top-1 acc	MACs (x 1e9)		#params x 1e7	
			inference	trainable	inference	trainable
tr18 baseline	-	60.42	2.22	1.13	1.13	
tr10	tr10	60.58 ± 0.04	1.48	0.96	9.39	
	tr18	63.38 ± 0.05	2.09	1.55	21.2	
tr34 baseline	-	63.39	4.64	2.14	2.14	
tr18	tr10	64.46 ± 0.05	2.69	1.59	9.39	
	tr18	66.26 ± 0.05	3.30	2.18	21.2	
tr50 baseline	-	63.24	5.19	2.39	2.39	
tr34	tr10	66.42 ± 0.15	5.11	2.60	9.39	

Table 1: Main CIFAR-100 (*left*) and tiny-ImageNet (*right*) results. Each number is reported over three random seeds. All settings have 20 experts, whose first three blocks are the (frozen) layers of the base model. We report accuracy and efficiency metrics (number of operations and number of parameters) across various base and experts architectures.

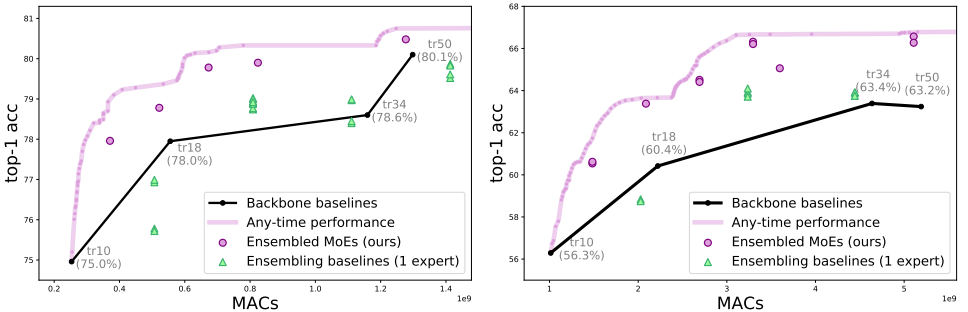


Figure 2: Accuracy vs MACs performance of our “anytime” variant models using a simple thresholding rule on CIFAR-100 (*left*) and tiny-ImageNet (*right*).

using fewer training iterations (200 epochs for CIFAR100, 100 for tiny-ImageNet and 40 for ImageNet). The features of the base model are kept frozen.

In this section, to assess the benefits of our proposed model and training scheme, we compare our proposed method to (i) the backbone models at different depths, (ii) an ensembling baseline with equivalent computational cost, (iii) hierarchical classification, and (iv) two recent dynamic routing works [43, 67]. We also report results of an ablation experiment on using different ensembling methods. Finally, we report detailed hyperparameters used for the experiments, and further ablations in the supplemental material.

4.1 Results on Small and Medium-scale Datasets

We first report results on CIFAR-100 and tiny-ImageNet for tiny-ResNets of different depths in Table 1. All results are reported with 20 experts, branching off the base model after the third residual block, and *without any early-exiting or dynamic ensembling*. These results show that even simple single-gate MoE can significantly improve the efficiency/accuracy trade-off over standard CNNs: Our proposed method consistently outperforms the backbone network for an equivalent MAC count. The only downside is that MoE generally has a higher parameter count at training time. Nevertheless, our asynchronous training scheme allows us to train experts independently across multiple devices efficiently. We also observe that using a deeper base model is often more beneficial than using deeper experts in terms of accuracy.

Comparison to ensembling. A natural baseline to compare to is to ensemble the base model with a unique “expert” trained on the whole dataset: The resulting model has the same cost as its MoE counterpart, minus the negligible cost of the linear layer gate. We also analyze the impact of the number of experts on the model: Adding more experts leads to higher specialization, but also more potential routing errors; thus, it is not evident that increasing the number of experts benefits the model. We report the corresponding results in Table 2: All MoE outperform the ensembling baseline, which shows the benefit of specialized experts. However, the impact of going from 10 to 20 experts is minimal: The benefit of splitting the data into specialized subsets starts to fade above 10 experts for these datasets.

tr18-tr18	CIFAR100	tiny-ImageNet
base model	77.95	60.42
baseline (1 expert)	78.99 \pm 0.29	63.83 \pm 0.08
5 experts	79.67 \pm 0.14	65.42 \pm 0.15
10 experts	79.84 \pm 0.13	65.72 \pm 0.17
20 experts	79.90 \pm 0.22	66.26 \pm 0.05

Table 2: Impact of the number of experts on the model accuracy and comparison to the ensembling baseline (equivalent to using only one expert in our model).

Anytime Inference Models. We explore the effect of the anytime inference model introduced in Section 2.3. To fully understand the scope of this dynamic behavior, we evaluate the accuracy of all models across various thresholds. We then plot the convex envelope of this set of curves, as shown in Figure 2. We observe that dynamically deciding for each sample whether to early exit through the base model or to use one or more experts consistently improves the overall accuracy/efficiency trade-off. Furthermore, this simple thresholding rule allows us to quickly adapt the model’s computational budget without retraining.

4.2 Results on ImageNet

Main results. We report results on ImageNet experiments for ResNet and MobileNet backbones in Table 3. Our previous observations still hold: The MoE model outperforms both the ensembling baseline and the backbone, and early-exiting based on the base model’s confidences helps further reduce computations for a limited drop in accuracy.

We also note that, unlike ResNet18, ResNet34’s MobileNetv3’s performance start to saturate and even slightly decreases with more experts. This behavior implies that the optimal number of experts is not only a property of the dataset but also of the architecture of both the experts and the base model.

ResNet18	None	$\tau = 0.75$	$\tau = 0.5$	None	$\tau = 0.75$	$\tau = 0.5$	None	$\tau = 0.75$	$\tau = 0.5$
baseline (1 expert)	71.50	71.50	71.13	74.33	74.29	74.00	68.06	68.13	68.15
4 experts	72.17	72.11	71.68	75.03	74.89	74.47	68.60	68.59	68.44
20 experts	72.38	72.38	71.73	75.05	74.92	74.56	68.58	68.53	68.46
MACs	2.64e9	2.18e9	2.03e9	5.64e9	4.42e9	4.06e9	8.13e7	6.83e7	6.36e7

(a) ResNet18 base model (**69.76%** accuracy, 1.82 GMACs) and experts

(b) ResNet34 base model (**73.31%**, 3.66 GMACs) and experts

(c) MobileNetv3-small base (**67.67%**, 5.65e7 MACs) and experts

Table 3: Main results on ImageNet. Experts share 3 layers in the ResNet experiments, and 8 in the MobileNet ones (half of the model in both case). We report our main results in the first column, without any early-exiting or dynamic ensembling. In the following columns, we report additional results with early-exiting obtained with different values of the threshold τ on the base model confidence.

Comparison to Dynamic Routing baselines. In this section, we compare our model to two recent dynamic routing works. In Table 4 (left) we compare to DeepMoE [43] on ImageNet: The model is a two-times wider ResNet-18 trained end-to-end with a sparsity constraint forcing the router in each layer to only activate roughly half of the channels for each sample. In Table 4 (right), we compare to RMN [52] on tiny-ImageNet: Each residual block is replicated 8 times (a total of 8^4 different computational paths), and for each, a routing based on a moving average of initial k-means centroids is learned. We could not compare directly to RMN on ImageNet as [52] uses a modified ResNet architecture including additional Squeeze&Excite [48] layers. Nevertheless, in terms of relative accuracy improvement and MACs, we observe that our model yields comparable trade-offs, despite using a single gate, hence significantly fewer computational paths. Furthermore, in contrast to both approaches, we can easily reach various computational budgets without retraining via early-exiting.

ImageNet Resnet-18	gates	acc.	MACs x1e9	#params (train) x1e9	tiny-ImageNet tr18	gates	base model	acc.	MACs	#params (train)
ours	1	72.17	2.64	5.10	ours (10 exp)	1	60.42	64.66	2.69e9	5.98e7
+early-exit $\tau = 0.75$	1	72.11	2.18	5.10	+ early-exit ($\tau = 0.75$)	1	60.42	64.58	2.44e9	5.98e7
DeepMoE [43]	17	70.95	1.81	7.02	RMN (no SE) [52]	5	61.78	64.30	2.22e9	9.02e7

Table 4: Comparison to recent dynamic routing literature. On the left, we compare our 4-experts ImageNet model with Wide-DeepMoE-18 from [43]. On the right, we compare our tr18-tr10 10 experts model with the tiny-ResNet18-based model of [52], excluding additional Squeeze&Excite layers. For [52], we also report the corresponding base model accuracy as we could not reproduce their baseline training results to use in our experiments.

4.3 Ablation experiments

In the supplemental material, we report further ablation experiments on (i) different early-exiting procedures and (ii) an alternative joint training based on Expectation-Maximization.

Per-sample vs per-class clustering initialization. Hierarchical classifiers are single-gated models whose routing is learned on a strict *per-class* basis. In the literature, the class taxonomy is either based on external knowledge [9, 13, 30, 35], clustering pretrained embeddings [34, 31], or jointly learned alongside the features [2]. We implement a per-class variant of our model, following the clustering process of [34, 31].

In Table 5, we show that per-sample routing always outperforms its per-class counterpart. Furthermore, we observe a significant accuracy gain if we re-evaluate the per-class model using the samples’ ground-truth classes as an oracle for predicting the correct expert. This indicates that learning the per-class routing is the main bottleneck. In fact, a sample (x, y) incorrectly mapped to an expert that has never seen class y is very detrimental to accuracy, even if this is partially compensated by the effect of ensembling. In contrast, per-sample routing allows several experts to gain knowledge about the same class and introduces a more flexible notion of diversity among experts.

top-1 acc	w/o ensembling	w/ ensembling
per-sample (ours)	63.11 \pm 0.11	65.72 \pm 0.10
per-class	62.48 \pm 0.13	63.85 \pm 0.08
per-class + oracle	68.8 \pm 0.10	67.99 \pm 0.04

Table 5: Comparison to hierarchical classification. We introduce a per-class variant of our model following [34, 31], and an oracle variant in which the gate follows the true class-to-expert distribution. Results are reported on tiny-ImageNet with 10 experts, in the tr18-tr18 configuration.

Analysing the Ensemblers’ performance

In Table 6, we compare results for different ensembling scheme with equivalent computation costs: Even without ensembling, MoE outperforms the base model. Nevertheless, all ensembling methods perform strictly better than trusting the selected expert only. Second, we observe that **stacking** and **bagging** always outperform ensembling the top-2 experts, which shows the benefit of ensembling with the base model rather than another specialized expert. We use **bagging** in our experiments as it is simpler, non-parametric, and does not require training.

base - expert	tr10-tr10	tr10-tr18	tr18-tr18
base model	56.29	56.29	60.42
no ensembling	57.80	59.53	63.82
top-2 experts	58.69	60.55	64.19
stacking	60.84	64.63	66.29
bagging	60.54	64.77	66.32

Table 6: Impact of the ensembler design on accuracy (tiny-ImageNet, 20 experts)

Qualitative Analysis of The Experts’ Specialization Pattern.

Finally, we qualitatively analyze the experts’ behavior: For each sample, we record which expert reaches minimal cross-entropy loss on that given sample. We then display the resulting class distribution across experts of the whole training set (see Appendix 3): The experts do end up specializing to specific subsets of the data, although, in contrast to hierarchical classification, many classes are still clearly split across several experts. Furthermore, most of these specialization patterns are consistent across the number of experts. Finally, while some experts clearly account for more classes than others, no expert is ever fully inactive. Looking more closely at the routed samples, we also see that the router uncovers natural intra-class variations, as illustrated for the class king penguin in Figure 3: The class king penguin is split across (i) close-up images where the orange beak is very visible, and end up being mapped to the same expert as oranges, bellpepper etc, which it is often confused with, and (ii) far away images which are instead grouped with other animal classes.



(a) The class king-penguin (left) co-occurs with other animals (right) for full-view images...



(b) ... but is often grouped with e.g., bell pepper when the image is a close-up view of its orange beak.

Figure 3: Per-sample routing uncovers meaningful intra-class modes.

5 Conclusions

In this work, we revisit the single-gate Mixture of Experts (MoE) for convolutional architectures. Specifically, we augment MoE with a novel ensembling scheme and a simple asynchronous and stable training pipeline leveraging a clustering-based initialization. Our model consistently reaches higher accuracy than hierarchical classifiers and a 1-expert ensembling baseline, revealing the benefits of training specialized experts with per-sample routing. Moreover, maintaining the base model as an independent branch allows us to further save computations at inference time using a simple threshold-based conditional rule.

Finally, our model is competitive with recent multi-layer MoE dynamic routing works, despite a smaller number of routers and experts, and provides a more lightweight and stable training pipeline. In the future, we plan to further improve our model’s training efficiency by investigating different sampling strategies based on the gate outputs.

References

- [1] Karim Ahmed and Lorenzo Torresani. BranchConnect: Image categorization with learned branch connections. In *IEEE Winter Conference on Applications of Computer Vision (WACV)*, 2018.
- [2] Karim Ahmed, Mohammad Haris Baig, and Lorenzo Torresani. Network of experts for large-scale image categorization. In *European Conference on Computer Vision (ECCV)*, 2016.
- [3] Yoshua Bengio, Nicholas Leonard, and Aaron Courville. Estimating or propagating gradients through stochastic neurons for conditional computation. *ArXiv*, abs/1308.3432, 2013.
- [4] Luca Bertinetto, Romain Mueller, Konstantinos Tertikas, Sina Samangooei, and Nicholas A. Lord. Making better mistakes: Leveraging class hierarchies with deep networks. In *Conference on Computer Vision and Pattern Recognition (CVPR)*, 2020.
- [5] Shaofeng Cai, Yao Shu, and Wei Wang. Dynamic routing networks. In *IEEE Winter Conference on Applications of Computer Vision (WACV)*, 2021.
- [6] Xinshi Chen, Hanjun Dai, Yu Li, Xin Gao, and Le Song. Learning to stop while learning to predict. In *International Conference on Machine Learning (ICML)*, 2020.
- [7] Aidan Clark, Diego de Las Casas, Aurelia Guy, Arthur Mensch, Michela Paganini, Jordan Hoffmann, Bogdan Damoc, Blake A. Hechtman, Trevor Cai, Sebastian Borgeaud, George van den Driessche, Eliza Rutherford, Tom Hennigan, Matthew Johnson, Katie Millican, Albin Cassirer, Chris Jones, Elena Buchatskaya, David Budden, Laurent Sifre, Simon Osindero, Oriol Vinyals, Jack W. Rae, Erich Elsen, Koray Kavukcuoglu, and Karen Simonyan. Unified scaling laws for routed language models. *ArXiv*, abs/2202.01169, 2022.
- [8] Arthur P. Dempster, Nan M. Laird, and Donald B. Rubin. Maximum likelihood from incomplete data via the EM. In *Journal of the Royal Statistical Society*, 1977.
- [9] Terrance Devries and Graham W. Taylor. Improved regularization of convolutional neural networks with cutout. *ArXiv*, abs/1708.04552, 2017.
- [10] David Eigen, Marc’Aurelio Ranzato, and Ilya Sutskever. Learning factored representations in a deep mixture of experts. In *Workshops of the International Conference on Learning Representations (ICLR)*, 2014.
- [11] William Fedus, Barret Zoph, and Noam Shazeer. Switch transformers: Scaling to trillion parameter models with simple and efficient sparsity. *ArXiv*, abs/2101.03961, 2021.
- [12] Gildenblat, J. and contributors. Pytorch library for cam methods. <https://github.com/jacobgil/pytorch-grad-cam>, 2021.
- [13] Wonjoon Goo, Juyong Kim, Gunhee Kim, and Sung Ju Hwang. Taxonomy-regularized semantic deep convolutional neural networks. In *European Conference on Computer Vision (ECCV)*, 2016.

- [14] Sam Gross, Marc’Aurelio Ranzato, and Arthur D. Szlam. Hard mixtures of experts for large scale weakly supervised vision. In *Conference on Computer Vision and Pattern Recognition (CVPR)*, 2017.
- [15] Chuan Guo, Geoff Pleiss, Yu Sun, and Kilian Q. Weinberger. On calibration of modern neural networks. In *International Conference on Machine Learning (ICML)*, 2017.
- [16] Kaiming He, X. Zhang, Shaoqing Ren, and Jian Sun. Deep residual learning for image recognition. In *Conference on Computer Vision and Pattern Recognition (CVPR)*, 2016.
- [17] Andrew G. Howard, Mark Sandler, Grace Chu, Liang-Chieh Chen, Bo Chen, Mingxing Tan, Weijun Wang, Yukun Zhu, Ruoming Pang, Vijay Vasudevan, Quoc V. Le, and Hartwig Adam. Searching for MobileNetV3. In *International Conference on Computer Vision (ICCV)*, 2019.
- [18] Jie Hu, Li Shen, Samuel Albanie, Gang Sun, and Enhua Wu. Squeeze-and-Excitation networks. *IEEE Transactions on Pattern Analysis and Machine Intelligence (T-PAMI)*, 2020.
- [19] Gao Huang, Danlu Chen, Tianhong Li, Felix Wu, Laurens van der Maaten, and Kilian Q. Weinberger. Multi-scale dense networks for resource efficient image classification. In *International Conference on Learning Representations (ICLR)*, 2018.
- [20] Hyo Jin Kim and Jan-Michael Frahm. Hierarchy of alternating specialists for scene recognition. In *European Conference on Computer Vision (ECCV)*, 2018.
- [21] Jang-Hyun Kim, Wonho Choo, and Hyun Oh Song. Puzzle Mix: Exploiting saliency and local statistics for optimal mixup. In *International Conference on Machine Learning (ICML)*, 2020.
- [22] James Kirkpatrick, Razvan Pascanu, Neil C. Rabinowitz, Joel Veness, Guillaume Desjardins, Andrei A. Rusu, Kieran Milan, John Quan, Tiago Ramalho, Agnieszka Grabska-Barwinska, Demis Hassabis, Claudia Clopath, Dharshan Kumaran, and Raia Hadsell. Overcoming catastrophic forgetting in neural networks. In *Proceedings of the National Academy of Sciences*, 2017.
- [23] Alex Krizhevsky. Learning multiple layers of features from tiny images. In *Thesis*, 2009.
- [24] H. Lee, S. Eum, and H. Kwon. ME R-CNN: Multi-expert R-CNN for object detection. *IEEE Transactions on Image Processing*, 29:1030–1044, 2020.
- [25] Dmitry Lepikhin, HyoukJoong Lee, Yuanzhong Xu, Dehao Chen, Orhan Firat, Yanping Huang, Maxim Krikun, Noam Shazeer, and Zhifeng Chen. GShard: Scaling giant models with conditional computation and automatic sharding. In *International Conference on Learning Representations (ICLR)*, 2021.
- [26] Fei Li, Andrej Karpathy, and Justin Johnson. Tiny-ImageNet visual recognition challenge. <https://www.kaggle.com/c/tiny-imagenet>, 2017.
- [27] Siyuan Li, Zicheng Liu, Di Wu, Zihan Liu, and Stan Z. Li. Boosting discriminative visual representation learning with scenario-agnostic mixup. *ArXiv*, abs/2111.15454, 2021.

- [28] Xiaoni Li, Yucan Zhou, Yu Zhou, and Weiping Wang. MMF: Multi-task multi-structure fusion for hierarchical image classification. In *International Conference on Artificial Neural Networks (ICANN)*, 2021.
- [29] J. MacQueen. Some methods for classification and analysis of multivariate observations. In *Berkeley Symposium on Mathematical Statistics and Probability*, 1967.
- [30] Marcin Marszalek and Cordelia Schmid. Constructing category hierarchies for visual recognition. In *European Conference on Computer Vision (ECCV)*, 2008.
- [31] Mason McGill and Pietro Perona. Deciding how to decide: Dynamic routing in artificial neural networks. In *International Conference on Machine Learning (ICML)*, 2017.
- [32] George A. Miller, Richard Beckwith, Christiane D. Fellbaum, Derek Gross, and Katherine J. Miller. Introduction to WordNet: An on-line lexical database. *International Journal of Lexicography*, 1990.
- [33] Matthias Minderer, Josip Djolonga, Rob Romijnders, Frances Ann Hubis, Xiaohua Zhai, Neil Houlsby, Dustin Tran, and Mario Lucic. Revisiting the calibration of modern neural networks. In *Conference on Neural Information Processing Systems (NeurIPS)*, 2021.
- [34] Ravi Teja Mullapudi, William R. Mark, Noam M. Shazeer, and Kayvon Fatahalian. HydraNets: Specialized dynamic architectures for efficient inference. In *Conference on Computer Vision and Pattern Recognition (CVPR)*, 2018.
- [35] Joan Puigcerver, Carlos Riquelme, Basil Mustafa, Cédric Renggli, André Susano Pinto, Sylvain Gelly, Daniel Keysers, and Neil Houlsby. Scalable transfer learning with expert models. In *International Conference on Learning Representations (ICLR)*, 2021.
- [36] Pytorch. Torchvision model zoo. <https://pytorch.org/vision/stable/models.html>, 2022.
- [37] Pytorch. Torchvision models training hyperparameters. <https://github.com/pytorch/vision/tree/main/references/classification>, 2022.
- [38] Vinay V. Ramasesh, Ethan Dyer, and Maithra Raghu. Anatomy of catastrophic forgetting: Hidden representations and task semantics. In *International Conference on Learning Representations (ICLR)*, 2021.
- [39] Yongming Rao, Jiwen Lu, Ji Lin, and Jie Zhou. Runtime network routing for efficient image classification. *IEEE Transactions on Pattern Analysis and Machine Intelligence (T-PAMI)*, 2019.
- [40] Carlos Riquelme, Joan Puigcerver, Basil Mustafa, Maxim Neumann, Rodolphe Jenatton, André Susano Pinto, Daniel Keysers, and Neil Houlsby. Scaling vision with sparse mixture of experts. In *Conference on Neural Information Processing Systems (NeurIPS)*, 2021.
- [41] Clemens Rosenbaum, Ignacio Cases, Matthew Riemer, and Tim Klinger. Routing networks and the challenges of modular and compositional computation. *ArXiv*, abs/1904.12774, 2019.

- [42] Olga Russakovsky, Jia Deng, Hao Su, Jonathan Krause, Sanjeev Satheesh, Sean Ma, Zhiheng Huang, Andrej Karpathy, Aditya Khosla, Michael S. Bernstein, Alexander C. Berg, and Li Fei-Fei. ImageNet large scale visual recognition challenge. *International Journal of Computer Vision (IJCV)*, 2015.
- [43] Simone Scardapane, Danilo Comminiello, Michele Scarpiniti, Enzo Baccarelli, and Aurelio Uncini. Differentiable branching in deep networks for fast inference. In *International Conference on Acoustics, Speech, and Signal Processing (ICASSP)*, 2020.
- [44] Joseph Sill, Gábor Takács, Lester W. Mackey, and David Lin. Feature-weighted linear stacking. *ArXiv*, abs/0911.0460, 2009.
- [45] S. Teerapittayanon, B. McDanel, and H. T. Kung. BranchyNet: Fast inference via early exiting from deep neural networks. In *International Conference on Pattern Recognition (ICPR)*, 2016.
- [46] A. F. M. Shahab Uddin, Mst Sirazam Monira, Wheemyung Shin, TaeChoong Chung, and Sung-Ho Bae. SaliencyMix: A saliency guided data augmentation strategy for better regularization. In *International Conference on Learning Representations (ICLR)*, volume abs/2006.01791, 2021.
- [47] Xin Wang, Fisher Yu, Zi-Yi Dou, and Joseph Gonzalez. SkipNet: Learning dynamic routing in convolutional networks. In *European Conference on Computer Vision (ECCV)*, 2018.
- [48] Xin Wang, Fisher Yu, Lisa Dunlap, Yian Ma, Yi-An Ma, Ruth Wang, Azalia Mirhoseini, Trevor Darrell, and Joseph Gonzalez. Deep mixture of experts via shallow embedding. In *Uncertainty in Artificial Intelligence (UAI)*, 2019.
- [49] Zuxuan Wu, Tushar Nagarajan, Abhishek Kumar, Steven J. Rennie, Larry S. Davis, Kristen Grauman, and Rogério Schmidt Feris. BlockDrop: Dynamic inference paths in residual networks. In *Conference on Computer Vision and Pattern Recognition (CVPR)*, 2018.
- [50] Ji Xin, Raphael Tang, Jaejun Lee, Yaoliang Yu, and Jimmy J. Lin. DeeBERT: dynamic early exiting for accelerating BERT inference. In *Annual Meeting of the Association for Computational Linguistics (ACL)*, 2020.
- [51] Zhicheng Yan, Hao Zhang, Robinson Piramuthu, Vignesh Jagadeesh, Dennis DeCoste, Wei Di, and Yizhou Yu. HD-CNN: Hierarchical deep convolutional neural networks for large scale visual recognition. In *International Conference on Computer Vision (ICCV)*, 2015.
- [52] Kaipeng Zhang, Zhenqiang Li, Zhifeng Li, Wei Liu, and Yoichi Sato. Neural routing by memory. In *Conference on Neural Information Processing Systems (NeurIPS)*, 2021.
- [53] Yikang Zhang, Zhuo Chen, and Zhao Zhong. Collaboration of experts: Achieving 80% top-1 accuracy on ImageNet with 100m FLOPs. *ArXiv*, abs/2107.03815, 2021.

Supplemental Material to BMVC2022

“Revisiting Single-gated Mixtures of Experts”

1 Datasets Detailed Description

We perform experiments on three datasets which we describe below:

- CIFAR-100 [23] (32x32 images, 50k training samples, 10k test samples, 100 classes) is a classic benchmark for small-scale image classification.
- tiny-ImageNet [26] (64x64 images, 100k training samples, 10k test samples, 200 classes) is a downscaled subset of ImageNet. It is significantly more challenging than CIFAR-100, which, combined with its reasonable scale, allows us to perform comprehensive ablation experiments in this study.
- ILSVRC2012 [24] (224x224 images, 1.28M training samples, 50k test samples, 1000 classes) is the de-facto benchmark for large-scale classification.

2 Training hyperparameters

In this section, we report the hyperparameters we used to train our baselines and run our experiments.

CIFAR-100. We follow the training pipeline of [9] to train our CIFAR-100 baselines. Each model is trained for **200** epochs with an initial learning of **0.1**; The learning rate is decayed by a factor of **5** at epoch **60**, **120** and **160**. The model is trained with SGD with a momentum of **0.9**. Finally, we use a batch size of **128**. For training the experts, we use the same hyperparameters, but train them with batch size **512** (4 times fewer training iterations), starting from pretrained weights from the base models.

tiny-ImageNet. We follow the training pipeline of [27] to train our tiny-ImageNet baselines. Each model is trained for **400** epochs with an initial learning of **0.2**; The learning rate is decayed by a factor of **10** at epoch **200** and **300**. The model is trained with SGD with a momentum of **0.9**. Finally, we use a batch size of **256**. For training the experts, we use the same hyperparameters, but only train for **100** epochs and the same batch size of 256, starting from pretrained weights from the base models.

ImageNet. We use the torchvision default pretrained models, whose training hyperparameters details can be found in [28]. We train all our experts with the same hyperparameters except (i) We use cosine learning rate decay and (ii) we use fewer training iterations (**45** epochs with batch size **2048** for our experts, versus **90** epochs with batch size **32** in the original ResNet18, and **600** epochs with batch size **128** in the original MobileNetv3-small).

3 Qualitative Analysis of Experts specialization

In this section, we report on a few qualitative results to highlight how the experts specialize during training. **First**, we perform a simple analysis on trained experts: For each sample, we record which expert reaches minimal cross-entropy loss on that given sample. We then display the resulting class distribution across experts of the whole training set. We report the results in [Figure 4](#): We observe that the experts do end up specializing to specific subsets of the data, although, in contrast to hierarchical classification, many classes are still clearly split across several experts. Furthermore, most of these specialization patterns are consistent across the number of experts. Finally, while some experts clearly account for more classes than others, no expert is ever fully inactive.

Second, we visualize the initial sample-to-expert assignment from the gate g_0 , following the K -means clustering step on the base model. We report some of these visualizations on ImageNet in [Figure 5](#). The initial gate does find meaningful groupings in the dataset, following the base model’s pretrained embeddings; Furthermore, the mapping does not exactly respect the dataset’s labels as most classes are distributed across more than one expert. Finally, we observe that there are different levels of "density" across the clusters: E.g. the 9-th expert is very self-contained and contains almost entirely all dog breeds. In contrast the 6-th expert contains many more varied classes, and not always fully, mostly composed of common household objects.

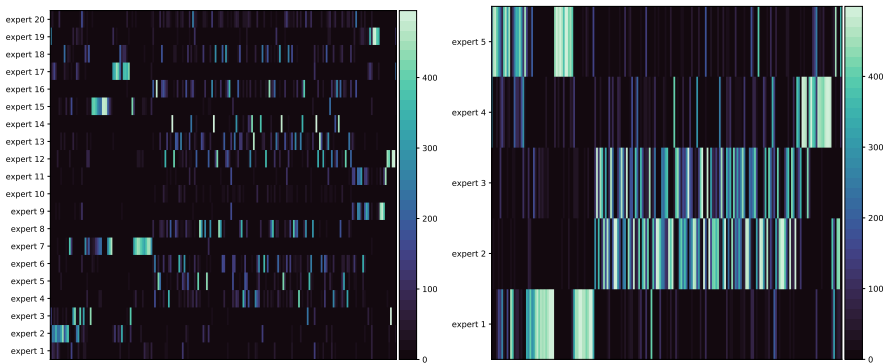
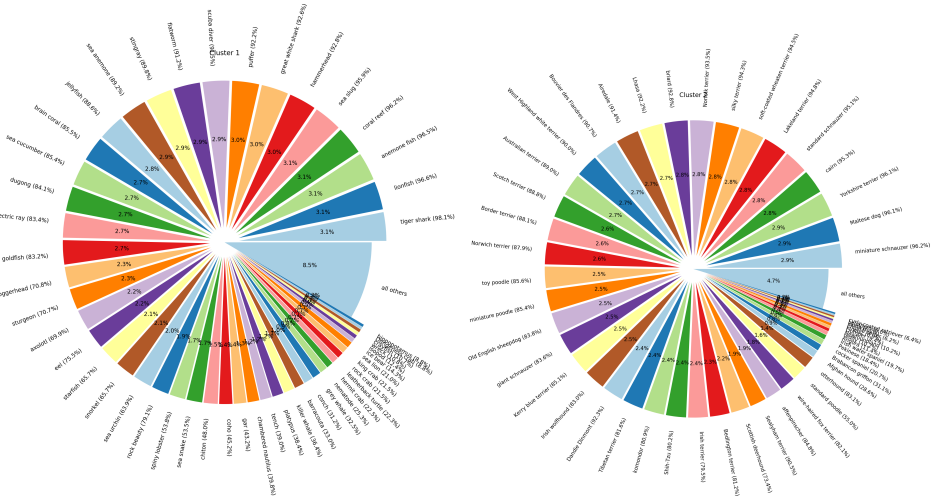


Figure 4: Specialization pattern of the trained experts for 20 experts (*left*) and 5 experts (*right*) on the tiny-ImageNet dataset. The x-axis represents the 200 classes, and the y-axis represents the experts. The cells’ colors represent the number of training samples of said class and for which said expert yields the lowest cross-entropy loss

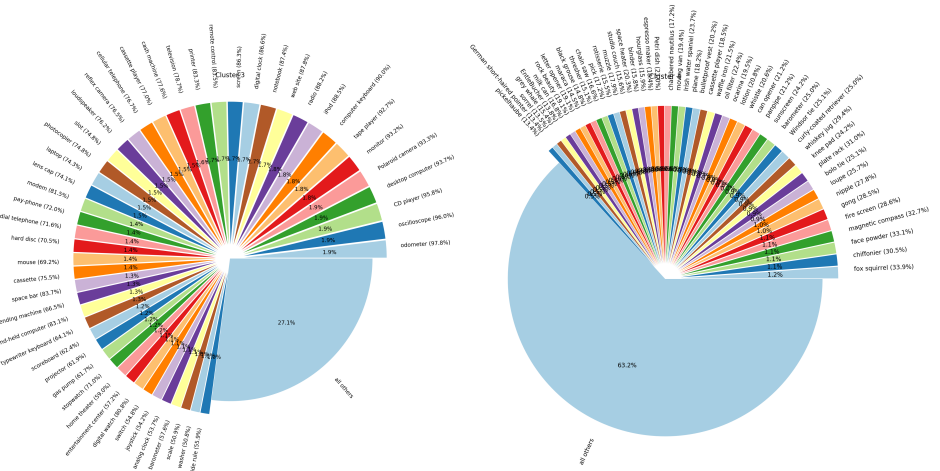
4 Analysis of the EM Training Scheme

As described using the EM algorithm allows us to jointly train the gate alongside the experts, while preserving some training stability. In particular, a determining factor is N_E , the number of E steps update. The higher this number is, the more often the gate is updated based on experts feedback. Our asynchronous training pipeline (Algorithm ‘) can be seen as a special case $N_E = 0$.

Given a fixed number of total epochs, n_e we vary the number of EM iterations, N_E . For our proposed training pipelines ($N_E = 0$) this means that the experts are trained for n_e epochs



(a) Example of two self-contained / highly specialized experts



(b) Example of complex experts with much higher class variation

Figure 5: Visualization of some sample-to-expert mappings from the precomputed initial gate g_0 on ImageNet for 20 experts and the ResNet18 base model. Each pie chart represents an expert; For readability, only the slices of the top-k classes are displayed individually. The percentage *inside* a slice is the percentage of this class among the samples mapped to this expert. Conversely, the percentage next to the class label is the percentage among all samples of the class (across all experts): A high percentage means that the class is almost entirely contained in one cluster. Best seen zoomed in.

with the fixed initial gate g_0 . For $N_E > 0$, the experts are also trained for n_e epochs, but every $\frac{n_e}{N_E+1}$ epoch, the gate weights are updated based on the current experts’ performance using the E step formula in **Equation 2**.

We report quantitative results on tiny-ImageNet in **Figure 6 (left)**, and observe that joint training does result in more accurate models. However, this makes training cumbersome as it requires synchronization across experts every time the E step is computed, i.e., a total of N_E times.

For the case of $N_E = 40$, we further analyse the difference between the initial gate g_0 and the learned gate g at the end of training, as shown in Figure 6: The two gates differ on roughly 14% of the training dataset, and the assignment differences are not random but follow a specific pattern across classes.

N_E	top-1-acc (w/o ensembling)	top-1 acc (w/ ensembling)
0 (ours)	63.11	65.72
10	63.46	65.74
20	63.58	65.84
40	64.48	66.15

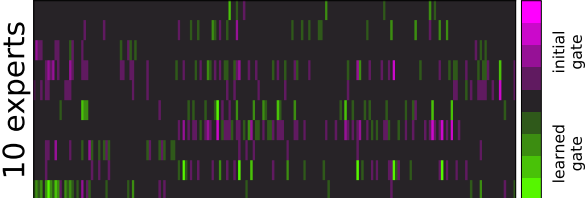


Figure 6: (left) Impact of increasing the number of E steps, N_E , when jointly training the gate and experts, using the setup of Table 1 (tiny-ImageNet, 10 experts). The total training budget is the same for all runs, only the number of updates differ. (right) We plot the heatmap of the difference between the class-to-expert assignments of the initial gate g_0 and the final trained gate for $N_E = 40$.

We also detail the five most consistent differences in assignment between these two gates below: The samples assigned to a different expert by the learned gate g are semantically meaningful: g often re-assigns the samples to an expert that already contained a large proportion of its ground-truth class.

- ✓ **40** samples of the class `steel arch bridge` and **105** samples of the class `triumphal arch` originally mapped to expert **4** by g_0 are mapped to expert **5** by the learned gate instead.
- ✓ **96** samples of the class `espresso` originally mapped to expert **6** by g_0 are mapped to expert **7** by the learned gate instead.
- ✓ **81** samples of the class `European Fire Salamander` originally mapped to expert **8** by g_0 are mapped to expert **1** by the learned gate instead.
- x **59** samples of the class `bikini` originally mapped to expert **2** by g_0 are mapped to expert **9** by the learned gate instead.

For reference, and to better understand each expert’s specialty, the most often assigned expert to each class by the original g_0 gate in this experiment was as follows:

- **Expert 1:** European fire salamander, bullfrog, tailed frog, American alligator, boa constrictor, trilobite, scorpion, tarantula, centipede, brain coral, slug, sea slug, spiny lobster, dugong, cockroach, sea cucumber, snorkel, coral reef
- **Expert 2:** academic gown, apron, bikini, bow tie, cardigan, Christmas stocking, fur coat, kimono, miniskirt, neck brace, plunger, poncho, potter’s wheel, punching bag, sock, sombrero, sunglasses, swimming trunks, teddy, vestment, ice lolly
- **Expert 3:** goose, koala, Chihuahua, Yorkshire terrier, golden retriever, Labrador retriever, German shepherd, standard poodle, tabby, Persian cat, Egyptian cat, cougar, lion, brown bear, guinea pig, hog, ox, bison, bighorn, gazelle, Arabian camel, orangutan, chimpanzee, baboon, African elephant, lesser panda

- **Expert 4:** abacus, altar, bannister, barbershop, brass, cash machine, chest, computer keyboard, confectionery, desk, dining table, freight car, organ, parking meter, pay-phone, refrigerator, rocking chair, scoreboard, sewing machine, space heater, turnstile, comic book
- **Expert 5:** black stork, albatross, barn, beacon, birdhouse, cannon, cliff dwelling, crane, dam, flagpole, fountain, gondola, lifeboat, obelisk, picket fence, pole, projectile, steel arch bridge, suspension bridge, thatch, triumphal arch, viaduct, water tower, alp, cliff, lakeside, seashore
- **Expert 6:** American lobster, frying pan, wok, plate, guacamole, ice cream, pretzel, mashed potato, cauliflower, bell pepper, orange, lemon, banana, pomegranate, meat loaf, pizza, potpie
- **Expert 7:** goldfish, jellyfish, king penguin, backpack, barrel, bathtub, beaker, beer bottle, binoculars, broom, bucket, candle, CD player, chain, drumstick, dumbbell, gasmask, hourglass, iPod, lampshade, magnetic compass, nail, oboe, pill bottle, pop bottle, reel, remote control, sandal, stopwatch, syringe, teapot, water jug, wooden spoon, espresso
- **Expert 8:** black widow, snail, ladybug, fly, bee, grasshopper, walking stick, mantis, dragonfly, monarch, sulphur butterfly, spider web, mushroom, acorn
- **Expert 9:** basketball, butcher shop, jinrikisha, lawn mower, maypole, military uniform, rugby ball, torch, umbrella, volleyball
- **Expert 10:** beach wagon, bullet train, convertible, go-kart, limousine, moving van, police van, school bus, sports car, tractor, trolleybus

5 Derivation of the EM Algorithm

We denote by X and Y the random variables associated to the input data (images and associated class labels respectively). We denote by Z the hidden variable associated to the index of the expert that image X is most likely associated to.

We are interested in the two following probability densities:

- $p(Z|X)$: The gate network routing a sample to an expert. This corresponds to the gate, $g(k|x)$, in our model.
- $p(Y|X, Z = k)$: The probability distribution over class labels output by the k -th expert. This corresponds to the expert, $e_k(y|x)$, in our model.

We are interested in maximizing the total likelihood of the model, $p(y|x)$ using Expectation-Maximization (**EM**). We first derive the Evidence lower bound (ELBO) on $p(y|x)$ using the standard variational Bayesian framework; Introducing the variational distribution $q(Z|X, Y)$, we have:

$$KL(q(z|x, y)||p(z|x, y)) = \mathbb{E}_q \log(q(z|x, y)) - \mathbb{E}_q \log p(z|x, y) \quad (4)$$

$$= \mathbb{E}_q \log(q(z|x, y)) - \mathbb{E}_q \underbrace{\log p(z, y|x)}_{\log p(z|x) + \log p(y|z, x)} + \underbrace{\mathbb{E}_q \log p(y|x)}_{=\log p(y|x)} \quad (5)$$

$$= KL(q(z|x, y)||p(z|x)) - \mathbb{E}_q \log p(y|x, z) + \log p(y|x) \quad (6)$$

Reordering the terms around, we have:

$$\log p(y|x) = \underbrace{\mathbb{E}_q \log p(y|x, z) - KL(q(z|x, y)||p(z|x))}_{ELBO} + \underbrace{KL(q(z|x, y)||p(z|x, y))}_{\geq 0} \quad (7)$$

The underlying idea of EM is a two step process in which we (i) minimize the difference between $\log p(y|x)$ and the ELBO (i.e., minimize the right-hand term in (11)) and (ii) maximize the ELBO (left-hand terms in (11)), usually until convergence. We then reiterate these two steps until satisfied.

E step: Minimize the difference between ELBO and the likelihood

For this we only have to compute the posterior distribution, i.e., set q to:

$$q(z|x, y) \leftarrow p(z|x, y) = \frac{p(z|x)p(y|z, x)}{p(y|x)} = \frac{p(z|x)p(y|z, x)}{\sum_z p(z'|x)p(y|z', x)} \quad (8)$$

$$q(z|x, y) \leftarrow \frac{g(z|x)e_z(y|x)}{\sum_z g(z'|x)e_{z'}(y|x)} \quad (9)$$

M - step: Maximize ELBO with the fixed q

$$ELBO = \mathbb{E}_{z \sim q(z|x, y)} \log p(y|x, z) - KL(q(z|x, y)||p(z|x)) \quad (10)$$

Using our model's notations (and a sum over the experts rather than an expectation), this means we have to maximize:

$$\sum_z [q(z|x, y) \log e_z(y|x) - KL(q(z|x, y)||g(z|x))] \quad (11)$$

Thus we exactly recover **Equations 2 and 3** from the main text

Equivalence to backpropagation. The separation of the E and M step is crucial for training stability: In the M step, the updates for the parameters of the gating function and the experts become decoupled entirely, hence can be trained independently. In fact, if we perform the E and M steps on the same batch of data, then we have by definition that $q(z|x, y) = p(z|x, y)$ on the current batch. Therefore, the right-hand KL divergence term in **Equation 11** is equal to 0, and the ELBO is equal to the total log-likelihood. Therefore, the EM algorithm simply becomes equivalent to directly minimizing the total log-likelihood $\log p(y|x)$ via backpropagation.

In other words, performing the E and M steps simultaneously is equivalent to directly training the gate and experts jointly with standard backpropagation. However, we observed many training instabilities using direct backpropagation (e.g. gate collapse), which also

seems to be the case in the literature as most works introduce ad-hoc losses (e.g. balancing loss term) when implementing joint training via backpropagation.

Intuitively, this means that EM essentially implements a delay in the parameter updates: We estimate the probability of the data-points belonging to each expert in the E step, and then we update the gate and expert functions following that estimate for a few epochs. The algorithm thus incurs one extra hyperparameter on top of standard backpropagation; That is, how many times we go through the E step to update the expert assignments estimates (we denote this hyperparameter as N_E in the main text).

6 Ablation: Expert Entry Layer

In the main paper, we always set the number of early layers shared by the experts to be about half the architecture (i.e. 3 layers for ResNet-based models, and 8 for MobileNetv3-small).

Performing a full ablation study on this parameter shows that it could be better optimized for further accuracy gain: For instance in [Figure 7](#), we observe that sharing 2 layers instead of 3 yields higher final accuracies on CIFAR-100. In both CIFAR-100 and tiny-ImageNet, we also see that there is a clear drop when the experts are reduced to only being linear layers. In general, we observe that the early features from the tiny-ImageNet base model are useful to the expert until a higher depth than the CIFAR ones. Automatically tuning this parameter for a given dataset and architecture is a research direction we consider for future work.

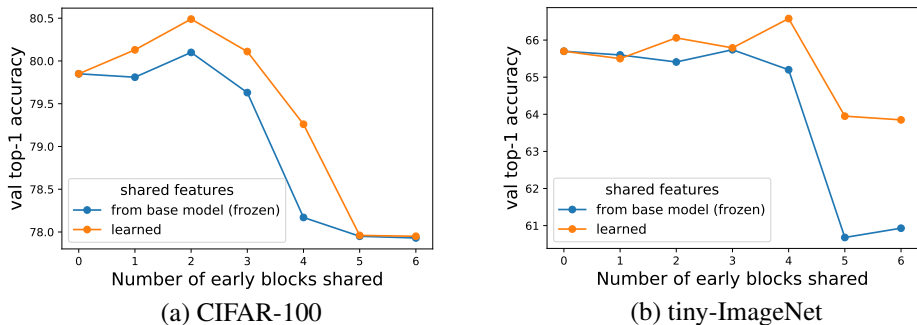


Figure 7: Validation accuracy when varying the number of early layers shared by the experts. All experiments were performed using 10 experts in the `tr18-tr18` configuration on CIFAR-100 (*left*) and tiny-ImageNet (*right*).

7 Ablation: γ Hyperparameter

In this section, we analyze the effect of the γ hyperparameter that we use to smooth the gate weights during training the experts, as described in [Section 2.2](#): γ can be interpreted as a non-zero weight given to all "negative samples" (those which the gate does not map to the current expert) while training an expert. In [Figure 8](#), we report accuracy results when varying γ . We observe that too low values of γ are detrimental to accuracy, both with and without ensemblers. However the model seems to be more robust to higher values of γ . In practice, we use a value $\gamma = 0.05$ for all our main experiments.

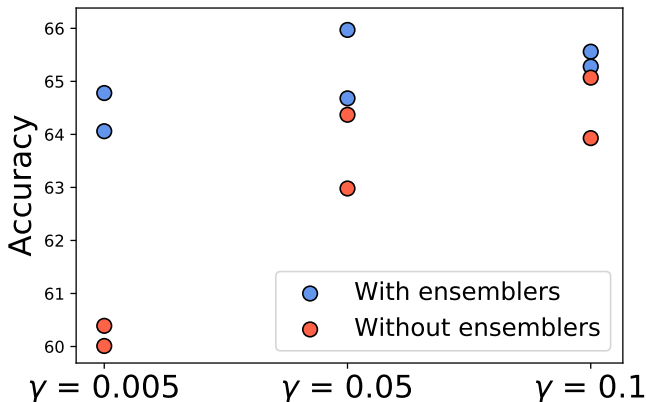


Figure 8: Effect of varying the γ hyper-parameter (lower bound of the gate clipping operation Γ when training the experts). Results are displayed for two random seeds, and obtained on tiny-ImageNet, for a `tr18-tr18` model with 10 experts.

8 Ablation: Early-exiting based on the gate or base model

Thresholding based rule. Our framework allows for two approaches to threshold-based early-exiting: (i) thresholding the gate’s confidence; and (ii) thresholding the base model’s confidence. Thresholding the gate’s confidence is based on the intuition that samples which are not routed confidently are also more likely to be classified wrong. On the other hand, base model thresholding directly builds on the intuition that the base model predicts correct samples with high confidence while samples with lower confidence are more likely to be classified wrong. Based on the reliability diagrams in Figure 9, we can see that, while not perfectly calibrated, there is a strong correlation between confidence and accuracy for the base model, while the same is not the case for the gate module. Therefore, we use the base model’s confidence rather than the gate’s as our guide for early-exiting in the main text and all experiments.

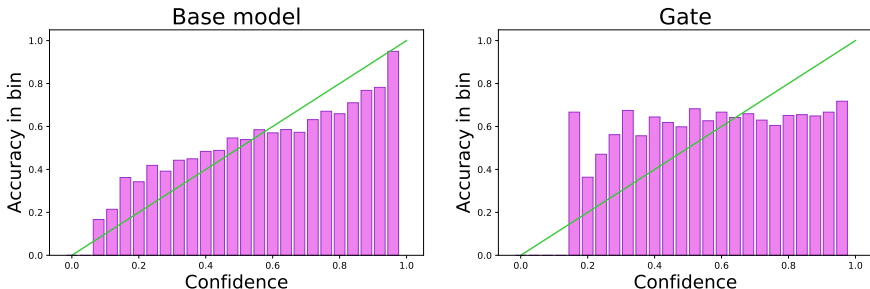


Figure 9: Reliability pattern for `tr10` on tiny-ImageNet (20 `tr-10` experts). The bins on the x-axis correspond to the confidence of the base model (*left*) and the gate (*right*). The y-axis corresponds to the accuracy on the samples in each bin.

To confirm this observations further, we also plot early-exiting results for both gate’s confidence thresholding and base model’s confidence thresholding for one of our models in Figure 10. We observe that base model thresholding indeed yields higher accuracy vs early-exiting ratio trade-offs.

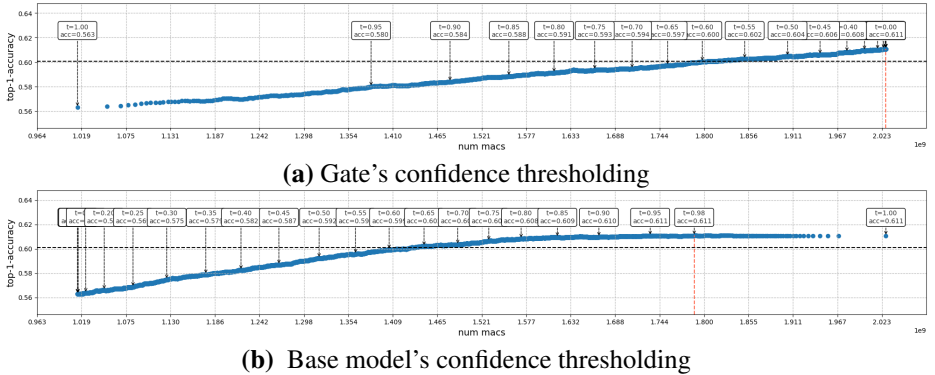


Figure 10: Comparison of early-exiting by thresholding either the gate’s confidence or the base model’s confidence for tr_{10} -base on tiny-ImageNet (20 tr_{10} experts). The x-axis corresponds to number of MACs at different threshold values. The y-axis corresponds to accuracy of model with early-exiting. Dashed *black* line corresponds to 1% accuracy drop. Dashed *red* line shows result for the best performing early-exiting threshold. Boxes above the blue curve show the different threshold values along with accuracy for each threshold.

Selecting the best threshold. We further report results for the best performing threshold in each setting in Table 7. We present results for tr_{10} -base on tiny-ImageNet (20 tr_{34} experts) and tr_{34} -base on tiny-ImageNet (20 tr_{10} experts). Looking at the whole range of thresholds allows us to find a model that fits the required computational budget. And selecting the best threshold by looking at the validation set can be seen as the upper bound. However, ideally, setting the optimal threshold properly and fairly would require an external validation holdout set. As an alternative, we use a subset of the training data to investigate whether we can set a threshold that generalizes well to inference time using training data only. We report the corresponding results in Table 7.

method	base - expert - num experts	baseline acc, % (no early-exiting)	early-exit ratio, %	top-1 acc, %	MACs (x 1e9)	#params (x 1e7)
validation-selection	tr10-tr34-20	66.22	20.11	66.27	4.7	2.2
	tr34-tr10-20	66.36	29.07	66.36	5.3	2.5
subset-selection	tr10-tr34-20	66.22	37.40	65.87	3.9	1.8
	tr34-tr10-20	66.36	75.07	65.18	4.9	2.3
gate-learning	tr10-tr34-20	66.22	10.64	65.54	5.1	2.4
	tr34-tr10-20	66.36	14.63	65.61	5.5	2.5

Table 7: Best performing thresholds for different approaches to early exiting as discussed in Appendix 8. Validation-selection stands for selecting optimal threshold on a validation set. Subset-selection stands for selection threshold on a subset of training data and using that for validation set. Gate learning stands for learning a separate gate for early exiting.

Learning the early-exiting gate. Alternatively, we can try to *train* the early-exiting behavior for a given early-exiting budget. This approach requires slightly changing model the architecture by adding another output to the gate g . We rewrite the early-exiting criterion to include this new output:

$$ee(x) = \mathbb{1}(\arg \max_k g(k|x) = K + 1) \quad (12)$$

where $\mathbb{1}$ is the indicator function, K is the number of experts, and the $K + 1$ index corresponds to the newly added early-exiting output. The drawback of such approach is that it requires to train additional parameters. However, since the rest of the network is kept fixed, training only requires a very small number of epochs and does not increase the complexity of the entire approach much.

Similar to previous works [8, 43], we use a supervised approach to train the new gate. However, unlike previous papers which use auxiliary classifiers to label each sample as being fit for early-exiting or not, we use a simple approach to label the data from the solution of an integer linear programming (ILP) problem: Specifically, we first fix an efficiency budget $\tau \in [0, 1]$, which is our target early exiting ratio on the training set. We then solve the optimal early exit assignment for budget τ on the training set by solving the following discrete optimization problem:

$$\text{maximize } \sum_{(x,y)} \left[ee(x) \phi(y|x) + (1 - ee(x)) \sum_{k=1}^K g(k|x) e'_k(y|x) \right]$$

subject to:

$$\begin{aligned} \frac{1}{N} \sum_x ee(x) &= \tau \\ \forall x, ee(x) &\in \{0, 1\} \end{aligned}$$

where N is the total number of samples, the assignment $ee(x) \in \{0, 1\}$ is 1 when sample x should early exit, and 0 otherwise. This is a simple ILP problem with binary variables, that directly solves the optimal assignment on the training set. Solving this problem yields binary labels $ee(x)$ which we then use to learn the early-exiting gate. We report accuracy results of the learned gate in Table 7. Overall, this approach seems to perform worse than selecting a simple threshold based on the training set, as the learned early exiting behavior does not generalize well at inference time⁴.